AIChE

Detailed Modeling of the Evaporation and Thermal Decomposition of Urea-Water Solution in SCR Systems

Vahid Ebrahimian, Andre Nicolle, and Chawki Habchi
IFP Energies nouvelles, 1–4, avenue de Bois-Préau, 92852 Rueil-Malmaison Cedex, France

DOI 10.1002/aic.12736
Published online August 30, 2011 in Wiley Online Library (wileyonlinelibrary.com).

This work is aimed to develop a multicomponent evaporation model for droplets of urea-water solution (UWS) and a thermal decomposition model of urea for automotive exhausts by using the selective catalytic reduction systems. In the multicomponent evaporation model, the influence of urea on the UWS evaporation is taken into account using a nonrandom two-liquid activity model. The thermal decomposition model is based on a semidetailed kinetic scheme accounting not only for the production of ammonia (NH_3) and isocyanic acid but also for the formation of heavier solid by-products (biuret, cyanuric acid, and ammelide). This kinetics model has been validated against gaseous data as well as solid-phase concentration profiles obtained by Lundstroem et al. (2009) and Schaber et al. (2004). Both models have been implemented in IFP-C3D industrial software to simulate UWS droplet evaporation and decomposition as well as the formation of solid by-products. It has been shown that the presence of the urea solute has a small influence on the water evaporation rate, but its effect on the UWS temperature is significant. In addition, the contributions of hydrolysis and thermolysis to urea decomposition have been assessed. Finally, the impacts of the heating rate as well as gas-phase chemistry on urea decomposition pathways have been studied in detail. It has been shown that reducing the heating rate of the UWS causes the extent of the polymerization to decrease because of the higher activation energy. © 2011 American Institute of Chemical Engineers *AIChE J,* 58: 1998–2009, 2012

Keywords: multicomponent, evaporation, UWS, Adblue, urea decomposition, thermolysis SCR, kinetics

Introduction

Selective catalytic reduction (SCR) is one of the most promising techniques for the abatement of the nitrogen oxides (NOx) emissions from lean-burn engines. For reasons of safety and toxicity, urea is the preferred selective reducing agent for mobile SCR applications.[1,2] Urea is typically being used as an aqueous solution at its eutectic composition (32.5% wt. urea, marketed as Adblue®).

In a typical SCR system, urea-water solution (UWS) is sprayed into the hot engine exhaust upstream of the SCR catalyst. It is commonly believed that water evaporates first,[3] and the remaining solid urea then melts and decomposes into gas phase ammonia (NH_3) and isocyanic acid (HNCO). However, urea decomposition in aqueous solution occurs in the same temperature range as water evaporation.[4]

Evaporation phenomena for hydrocarbons have been widely investigated experimentally and numerically during the past decades.[5–10] Evaporation of UWS is a little more complicated compared to the hydrocarbons evaporation due to the interaction of urea solute in water. When injected into the exhaust hot gases, UWS droplets undergo heating which leads to a progressive increase of urea concentration inside the droplet during the evaporation process. The effects of solute on evaporation of droplets have been studied by Basu and Cetegen.[11] They modeled liquid ceramic precursor droplets (composed of water and zirconium acetate) axially injected into plasma. As water evaporates, the concentration of solute augments which leads to the formation of a precipitate shell. They studied the effects of droplet size, shell porosity, and thickness, and they have shown different behaviors of droplet for different conditions. The same hypothesis could be applied to the UWS droplets. Dissolved urea affects the evaporation of water directly.[3,12,13] As the urea evaporation rate is very small relatively to that of water, the concentration of urea in the droplet increases. Two different scenarios may occur for the urea depending on the water evaporation rate. When the droplet size is small and/or the vaporization rate of water is low, the concentration of urea throughout the droplet increases uniformly which finally leads to the formation of a solid particle. However, when water vaporizes rapidly, urea concentration increases at the droplet surface which builds up an urea shell around the droplet. This may lead to the boiling of the water inside the urea shell and even to the explosion and fragmentation of the droplet as it has been observed in Ref.[14]. Although, this last scenario may occur for large droplets with high-heating rate, it is not considered in this work. In the presented UWS evaporation model, dissolved urea inside or at the droplet surface causes the vapor pressure of water to decrease which consequently decreases the evaporation rate of water compared to that of pure water.

Some authors[3,13] have considered the effect of urea on water vapor pressure. Birkhold et al.[3] used rapid mixing

Correspondence concerning this article should be addressed to A. Nicolle at andre.nicolle@ifpen.fr.

(RM) model to evaluate the influence of dissolved urea on the evaporation of water. In the RM model, infinite high transport coefficients are assumed for the liquid phase, resulting in spatial uniform temperature, concentration and fluid properties in the droplet, with the temporal change in quantities.[3,15,16] Kontin et al.[13] as well as Birkhold et al.[3] used the RM model for evaporation of water in UWS. They modified the standard gaseous-film model, proposed by Abramzon and Sirignano,[7] by introducing the mass flow-reduction coefficient proposed by Reinhold.[17] They proposed three different cases during the evaporation of water and enrichment of urea. In the oversaturated case, urea completely remains in solution; therefore, the possibility of an unlimited oversaturation is assumed. In the saturated case, a limited solubility is considered by precipitation of solid crystalline urea out of the liquid phase. In this case, the saturation pressure is described according to Raoult's law. In the crust case, a solid layer is formed at the particle surface during dissolution/evaporation which reduces the mass transfer. A reduction coefficient is then introduced in the evaporation rate expression and adjusted in their study, using an experimental investigation. This model gives relatively good results. However, an exact physical basis for the reduction coefficient would be required.

Several computational studies were carried out to predict UWS thermolysis. Abu-Ramadan et al.[18] studied the evaporation and thermolysis of UWS droplets. They modeled urea depletion from UWS either as a vaporization process or a direct thermolysis process from molten urea to ammonia and HNCO. The formation of by-products (biuret and heavier by-products) was neglected in their study. Birkhold et al.[3] found the RM model to have the best trade-off between accuracy and numerical effort. However, these studies did not consider the formation of deposits resulting from urea decomposition. Deposit formation can lead to backpressure generation, deterioration of the after-treatment system[19] and possible deactivation of the SCR catalyst.[20]

Numerous studies[21–24] indicate that urea decomposes readily in aqueous solution, yielding cyanate (NCO^-) and ammonium (NH_4^+) ions. The preferred reaction route seems to go through a zwitterionic intermediate, H_3NCONH.[25]

The hypothesis of hydrolysis of HNCO taking place in gas phase[26] seems not to be realistic as HNCO(g) is quite stable in the gas phase.[27–29] However, in solution, cyanate can be readily hydrolyzed to ammonia and carbon dioxide according to the sequence of reactions

$$NCO^- + H_2O(l) \rightarrow NH_2CO_2^- \ (aq) \ (R11a) \quad (1)$$

$$NH_2CO_2^- \ (aq) + H_2O \ (l) \rightarrow NH_3 \ (g) + HCO_3^- \ (aq) \ (R11b) \quad (2)$$

$$HCO_3^- \ (aq) + H^+(aq) \rightarrow H_2O(l) + CO_2 \ (g) \ (R11c) \quad (3)$$

Carbamate $NH_2CO_2^-$ ion was identified by Schoppelrei et al.[30] Although a nucleophilic addition of hydroxide to the carbon of HNCO was suggested by Kemp and Kohnstam,[31] a mechanism involving two water molecules attacking its C=N bond was recently proposed by Arroyo et al.[32]

The thermolysis of solid urea resulting from water evaporation from the UWS leads to the production of gaseous products (NH_3, HNCO) as well as heavier by-products (biuret, cyanuric acid (CYA), and ammelide). As in the case of urea in aqueous solution, the decomposition goes through the formation of NCO^- and NH_4^+.[33] The formation of biuret was suggested to involve the interaction of urea with NCO^- in the melt.[34] The presence of H_2O in gas phase seems to slightly affect solid urea decomposition.[35]

Alzueta et al.[36] proposed alternative channels for urea decomposition at very high temperature and pointed out some uncertainties in the HNCO gas-phase oxidation scheme. Recently, quantum chemical calculations[37] indicated that the most favorable urea decomposition pathway in gas phase leads to HNCO and NH_3.

In this study, the evaporation and thermal decomposition are numerically investigated. In the following section, an UWS evaporation model based on the multicomponent droplets evaporation model developed by the authors[10] is suggested. Next, a thermal decomposition model is presented. It is based on a semidetailed kinetic scheme accounting not only for the production of NH_3 and HNCO but also for the formation of heavier by-products (biuret, CYA, and ammelide).

Modeling

Evaporation modeling

In this work, a UWS droplet evaporation model is proposed, based on the multicomponent droplet evaporation model developed by the authors.[10] The suggested analysis is based on the conventional conservation equations of species and energy for the gas phase, and the energy balance equation at the liquid-gas interface. The species diffusion is based on the Hirschfelder law[38–40] rather than on the less general Fick's equation. Moreover, the heat flux due to species diffusion is taken into account in addition to the classical conduction heat flux between the gas and the liquid droplets. The liquid phase analysis is based on the infinite thermal conductivity liquid phase model [i.e., RM model], which has been justified by a reasonably good agreement between the predicted and experimental results.[10] The model relies on the spherical droplet hypothesis with no interaction between droplets. The effects of radiation as well as Soret and Dufour effects are neglected. The one-third rule is used for the properties of the gaseous mixture in the film region around the droplet.[41] Gas-phase quasi-steadiness and isobaric assumptions are applied to the model. The resulting governing equations for the model consist of two-phase flow equations for the gas and liquid phases along with the thermodynamic equilibrium condition at the liquid-gas interface. The UWS droplets contain two individual components (i.e., water and urea) and require a two-component evaporation model. However, the evaporation rate of urea is negligible at atmospheric pressure compared to the evaporation rate of water. This behavior results from the very small vapor pressure of urea, especially at atmospheric pressure. Therefore, the two-component evaporation model has been simplified as follows: only water is evaporated using the single-component evaporation model where the UWS vapor pressure is obtained using the Raoult's law and the nonrandom two-liquid (NRTL) activity model.[42] Finally, it is worth to note that the NRTL activity model has been also integrated in the liquid film evaporation model developed by Desoutter et al.[43] in the same manner as for droplet evaporation. Thus, only the evaporation of UWS droplets will be presented in this article.

UWS evaporation model

The proposed UWS evaporation model will be referred as UWS-NRTL. It is described in this section including some

details of the activity coefficient calculations using the NRTL model.

Gas-Phase Governing Equations. Droplet evaporation models are generally based on the balance equations of mass, momentum and energy. In the mass balance equation of species resolution, it is assumed that there is no chemical reaction in the gaseous environment. This is a good assumption for urea and water species. There is almost no urea vapor in the gaseous environment due to its very low-evaporation rate. Besides, the reactions of gaseous species with water vapor are negligible at low temperatures.[44,45] The gas-phase governing equations are used to obtain the mass flow rate and heat flux from the gas to the liquid. These quantities for water evaporation are summarized in the following sections.

Mass Flow Rate. On the basis of previous works, some authors[7,46] have considered the gaseous boundary layer around the droplet to evaluate heat and mass fluxes. These models give the instantaneous droplet vaporization rate from the integration of the quasi-steady species balance around the droplet. The mass evaporation rate for single-component water droplet is presented as:[10]

$$\dot{m} = \frac{2\pi r_{\mathrm{d}} \rho_{\mathrm{g}} \left\{ \hat{D}^{s}_{\mathrm{wg}} Sh_{\mathrm{w}} \left(Y^{s}_{\mathrm{w}} - Y^{\infty}_{\mathrm{w}} \right) - Y^{s}_{\mathrm{w}} \sum_{i=1}^{N} \hat{D}^{s}_{ig} Sh_{i} \left(Y^{s}_{i} - Y^{\infty}_{i} \right) \right\}}{1 - Y^{s}_{\mathrm{w}}} \tag{4}$$

where a modified diffusion coefficient is defined as follows:

$$\hat{D}_{ig} = D_{ig} \left[1 - X_i + Y_i \sum_{\substack{k=1 \\ k \neq i}}^{N} \frac{X_k}{Y_k} \right] \tag{5}$$

And, r_d is the droplet radius, Y_i^s and Y_i^∞ correspond respectively to the mass fraction of species i at the droplet surface (superscript s) and at infinity. X_i^s is the mole fraction of species i at the droplet surface. ρ_{g} and D_{ig} are the density and binary diffusion coefficient of species i into the gas mixture (index g). The dimensionless Sherwood number is defined as the ratio of the mass fraction gradient at the droplet surface and the average mass fraction gradient:

$$\mathrm{Sh} = -\frac{2r_{\mathrm{d}} \left. \frac{\partial Y}{\partial r} \right|_{r=r_{\mathrm{d}}}}{Y^{\mathrm{s}} - Y^{\infty}} \tag{6}$$

To consider the effect of natural convection due to volume forces such as the buoyancy force in the gravity field, the following relation is used for the Sherwood number:

$$\mathrm{Sh} = 2.0009 + 0.514 \left(\max \left(\mathrm{Re},\ \max(Gr, 0)^{1/2} \right) \right)^{1/2} \mathrm{Sc}^{1/3} \tag{7}$$

The Eq. 7 is the Kulmala–Vesala correlation[47] where the Grashof number (Gr) has been introduced along with the Reynolds number (Re) and the Schmidt number (Sc) by:

$$\mathrm{Re} = \frac{\rho_{\mathrm{g}} r_{\mathrm{d}}^2 V_{\mathrm{rel}}}{\mu_{\mathrm{g}}} \quad , \qquad Sc = \frac{\mu_{\mathrm{g}}}{\rho_{\mathrm{g}} D_{\mathrm{g}}} \quad , \qquad \mathrm{Gr} = \frac{8 g_0 r_{\mathrm{d}}^3 (T^{\infty} - T_{\mathrm{d}})}{(\upsilon^{\infty})^2 T^{\infty}} \tag{8}$$

V_{rel} is the relative velocity between the gas and droplet, $\mu_{,\mathrm{g}}$ is the dynamic viscosity in the gas mixture of the gaseous-film region, g_0 is the gravity acceleration, T^∞ and υ^∞ are the gas temperature and kinematic viscosity at infinity, T_{d} is the droplet temperature. The Grashof number arises in the study of situations involving natural convection. This phenomenon may occur at the entrance of the SCR system, for instance. It is important to note that the physical parameters in the gaseous-film region (with index g) are evaluated at the reference temperature[41]:

$$T_{\mathrm{ref}} = T_{\mathrm{d}} + A_{\mathrm{r}} (T^{\infty} - T_{\mathrm{d}}) \tag{9}$$

where, A_{r} is the averaging parameter. It has been shown by the authors[10] that the one-third rule ($A_{\mathrm{r}} = 1/3$) gives better results than the arithmetic mean rule ($A_{\mathrm{r}} = 1/2$).

Gaseous Heat Flux. During the evaporation process of a droplet, the internal energy of the surrounding gas and its composition evolve simultaneously. In this study, the heat flux in the gas phase comprises the contributions of the thermal conduction flux and the compositional changes resulting from species diffusion:

$$Q_{\mathrm{g}} = 2\pi r_{\mathrm{d}} \lambda_{\mathrm{g}}\, Nu (T^{\infty} - T_{\mathrm{d}}) - \dot{m} h_{\mathrm{g}} \left(1 - Y^{\mathrm{s}}_{\mathrm{w}} \right) \tag{10}$$

where, λ_g is the heat conduction coefficient, h_{g} (J kg^{-1}) is the specific enthalpy of the vapor at T_{ref} and Nu is the dimensionless Nusselt number defined as:

$$\mathrm{Nu} = -\frac{2r_{\mathrm{d}} \left. \frac{\partial T}{\partial r} \right|_{r=r_{\mathrm{d}}}}{T_{\mathrm{d}} - T^{\infty}} \tag{11}$$

Following Kulmala and Vesala[47] for the Sherwood number correlation , the Nusselt number is defined similarly by:

$$\mathrm{Nu} = 2.0009 + 0.514 \left(\max \left(\mathrm{Re}, \max(\mathrm{Gr}, 0)^{1/2} \right) \right)^{1/2} \mathrm{Pr}^{1/3} \tag{12}$$

where the Prandtl number, Pr is the defined as:

$$\mathrm{Pr} = \frac{C_{\mathrm{pg}} \mu_{\mathrm{g}}}{\lambda_{\mathrm{g}}} \tag{13}$$

and $C_{p\mathrm{g}}$ is the specific heat of the gas mixture in the gaseous-film region at constant pressure.

Liquid-Phase Energy Equation. As discussed above, droplet surface temperature is assumed to be equal to the mean temperature of the droplet ($T^s = T_{\mathrm{d}}$). The energy conservation equation for the two-phase system consisting of the droplet and the surrounding gas mixture allows evaluating the change in liquid droplet energy as:

$$m_{\mathrm{d}} C_{\mathrm{pf}} \frac{dT_{\mathrm{d}}}{dt} = Q_{\mathrm{l}} \tag{14}$$

where, m_{d} is the droplet mass, $C_{p\mathrm{f}}$ is the specific heat of liquid at constant pressure, T_{d} is the temperature of the droplet and Q_{l} (J s^{-1}) is the heat penetrating into the liquid phase. The energy balance at the liquid-gas interface could be written as:

$$Q_{\mathrm{l}} = Q_{\mathrm{g}} - \dot{m} L_{\mathrm{v,g}} \tag{15}$$

where, Q_{g} (J s^{-1}) is the heat flux from the gas to the liquid given by Eq. 10. $\dot{m}$ (kg s^{-1}) is the evaporation mass flow rate given by Eq. 4, and $L_{\mathrm{v,g}}$ (J kg^{-1}) is the mean latent heat of vaporization of water in the gaseous film region around the droplet.

Table 1. Binary Interaction Parameters for NRTL Model for Urea-Water Solution[42]

Parameters	c_{ij}	α_{ij}	a_{12}	a_{21}	b_{12}	b_{21}
Values	0	0.3	7.659	−1.536	−1463	−56.67

Determination of UWS Vapor Pressure. The evaporation of droplet consists of resolving two phase flow equations as well as satisfying the thermodynamic equilibrium condition at the liquid-gas interface. This equilibrium is based on the assumption that at the liquid-gas interface, the chemical potential for liquid and gas phases are equal for each species i. The evaporation model for UWS is based on the hypothesis that the vapor pressure of the water changes with the change in the concentration of urea in the solution. The properties of highly nonideal liquid solutions such as UWS could be estimated with the NRTL activity model. This model takes into account the interactions between the molecules in the liquid phase through the activity coefficient. The activity coefficient γ enables us to modify the fugacity of species in liquid phase.

For a liquid mixture which is in equilibrium with a vapor mixture at the same temperature and pressure, the thermodynamic equilibrium condition for every component i in the mixture is given by the fugacity.

$$f_i^{\mathrm{L}} = f_i^{\mathrm{V}} \tag{16}$$

where, f is the fugacity, and the exponents L and V represent the liquid and vapor phases, respectively. The fugacity of liquid phase for every component could be written as[48]:

$$f_i^{\mathrm{L}} = X_i^{\mathrm{L}} \gamma_i P_i^{\sigma}(T) \tag{17}$$

and for the vapor phase as:

$$f_i^{\mathrm{V}} = X_i^{\mathrm{V}} P \tag{18}$$

In the above equations, X_i^{L} and X_i^{V} are the mole fraction of species i in the liquid and vapor phases respectively. P_i^{σ} is the vapor pressure of component i, and P is the pressure at temperature T.

It should be noted that Eqs. 17 and 18 are written using the hypothesis that the vapor phase behaves as an ideal solution. This hypothesis is valid at low-pressure and high-temperature conditions. This choice is then justified in this work due to the high-temperatures and/or low-pressures conditions in the exhaust systems. The equality of the fugacities at equilibrium results in the following relationship:

$$X_i^{\mathrm{V}} P = X_i^{\mathrm{L}} \gamma_i P_i^{\sigma}\ (T) \tag{19}$$

In the case of UWS, the contribution of urea to the vapor pressure of the solution is extremely low. Then, urea mole fraction at liquid-gas interface can be assumed to be negligible (i.e. $X_u^V \approx 0$). However, the evaporation of water increases the contribution of urea in the UWS. For the liquid-vapor equilibrium of UWS, Eq. 19 could be simplified to the following relationship:

$$P = X_{\mathrm{w}}^{\mathrm{L}} \gamma_{\mathrm{w}} P_{\mathrm{w}}^{\sigma}(T) + X_{\mathrm{u}}^{\mathrm{L}} \gamma_{\mathrm{u}} P_{\mathrm{u}} \tag{20}$$

where the subscripts w and u represent water and urea, respectively. Because of the lack of data concerning the vapor pressure of pure urea, P_{u} is assumed to be equal to the sublimation pressure of urea. The extremely low values of the vapor pressure and sublimation pressure of the urea make it difficult to get the corresponding measured/estimated values of them. The DIPPR[49] proposes the following correlation for the sublimation pressure of urea:

$$\ln P_{\mathrm{u}} = 29.9548 - \frac{10876.1}{T} \tag{21}$$

where the pressure unit is Pa and the temperature unit is K.

NRTL Model. Like most of the activity models, NRTL[48] is a local composition model for calculating activity coefficients γ_i of species in a mixture with nonidealities. The NRTL model is presented with the following Eq. 22 where the indexes j and k sum over the total number of species in the mixture:

$$\ln \gamma_i = \frac{\sum_j \tau_{ji} G_{ji} X_j^L}{\sum_k G_{ki} X_k^{\mathrm{L}}} + \sum_j \frac{X_j^{\mathrm{L}} G_{ij}}{\sum_k G_{kj} X_k^L} \left(\tau_{ij} - \frac{\sum_k X_k^L \tau_{kj} G_{kj}}{\sum_k G_{kj} X_k^L} \right) \tag{22}$$

with:

$$\tau_{ij} = a_{ij} + \frac{b_{ij}}{T} + \frac{c_{ij}}{T^2} \tag{23}$$

$$G_{ji} = \exp\left(-\alpha_{ji} \tau_{ji}\right) \tag{24}$$

$$\alpha_{ji} = \alpha_{ij}{}' + \beta_{ij}{}' T \tag{25}$$

where X_j^{L} is the mole fraction of species i in the liquid phase. a_{ij}, b_{ij}, c_{ij}, a'_{ij}, and B'_{ij} are the binary interaction parameters of NRTL model. These parameters are regressed from experimental data on liquid-vapor for UWS[42] and presented in Table 1.

The activity coefficients for water and urea are then calculated from Eq. 22:

$$\gamma_{\mathrm{w}} = \exp\left\{ \left(X_{\mathrm{u}}^{\mathrm{L}}\right)^2 \left[\tau_{\mathrm{uw}} \left(\frac{G_{\mathrm{uw}}}{X_{\mathrm{w}}^{\mathrm{L}} + X_{\mathrm{u}}^{\mathrm{L}} G_{\mathrm{uw}}} \right)^2 + \left(\frac{\tau_{\mathrm{wu}} G_{\mathrm{wu}}}{\left(X_{\mathrm{u}}^{\mathrm{L}} + X_{\mathrm{w}}^{\mathrm{L}} G_{\mathrm{wu}}\right)^2} \right) \right] \right\} \tag{26}$$

$$\gamma_{\mathrm{u}} = \exp\left\{ \left(X_{\mathrm{w}}^{\mathrm{L}}\right)^2 \left[\tau_{\mathrm{wu}} \left(\frac{G_{\mathrm{wu}}}{X_{\mathrm{u}}^{\mathrm{L}} + X_{\mathrm{w}}^{\mathrm{L}} G_{\mathrm{wu}}} \right)^2 + \left(\frac{\tau_{\mathrm{uw}} G_{\mathrm{uw}}}{\left(X_{\mathrm{w}}^{\mathrm{L}} + X_{\mathrm{u}}^{\mathrm{L}} G_{\mathrm{uw}}\right)^2} \right) \right] \right\} \tag{27}$$

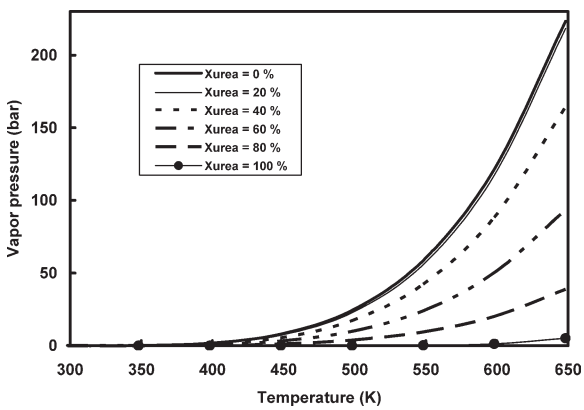

Figure 1. Vapor pressure diagram for urea-water solution at different temperatures and different mole fraction of urea in liquid phase.

Table 2. Condensed Phase Kinetic Scheme for Urea Thermal Decomposition

Reaction*	A_i (s^{-1})	E_i (kJ mol^{-1})	Refs.
(R1) urea $\rightarrow NH_4^+ + NCO^-$	8.50×10^6	84	21
(R2) $NH_4^+ \rightarrow NH_3(g) + H^+$	1.50×10^2	40	pw
(R3) $NCO^- + H^+ \rightarrow HNCO(g)$	6.57×10^2	10	pw
(R4) urea + $NCO^- + H^+ \rightarrow$ biuret	7.87×10^{14}	115	pw
(R5) biuret $\rightarrow$ urea + $NCO^- + H^+$	1.50×10^{24}	250	pw
(R6) biuret + $NCO^- + H^+ \rightarrow$ cya + $NH_3(g)$	2.81×10^{18}	150	pw
(R7) cya $\rightarrow 3\ NCO^- + 3\ H^+$	1.50×10^{19}	260	pw
(R8) cya + $NCO^- + H^+ \rightarrow$ ammelide + CO_2	3.48×10^5	35	pw
(R9) ammelide $\rightarrow 2\ NCO^- + 2\ H^+ + HCN(g) + NH(g)$	6.00×10^{14}	220	pw
(R10) urea (aq) $\rightarrow NH_4^+ + NCO^-$	1.20×10^8	84	21
(R11) $NCO^- + H^+ + H_2O$ (aq) $\rightarrow NH_3 + CO_2(g)$	5.62×10^9	59	21
(R12) urea (aq) + $NCO^- + H^+ \rightarrow$ biuret	3.93×10^{14}	115	pw

*aq stands for "aqueous" and cya for cyanuric acid. pw: present work.

The saturation pressure is obtained through Eq. 20 having the sublimation pressure of urea and vapor pressure of water, mole fraction, and activity coefficient of water. Figure 1 illustrates the result obtained for the saturation pressure of UWS over the range 298.15–647.3 K and for different urea mole fractions in the solution. According to Figure 1, the vapor pressure of UWS decreases by increasing the concentration of urea in the solution. As the mole fraction of urea reaches its highest value (when there is no more water in the UWS), the vapor pressure calculated from Eq. 20 is the vapor pressure of pure urea. This situation is also shown in Figure 1. As evaporation continues, the concentration of urea in the liquid increases, which may affects the heating and the evaporation of water from the UWS.

Evaporation Model Implementation. The above UWS Evaporation model (UWS-NRTL) is implemented in IFP-C3D industrial software.[50] An iterative method is needed for the implicit calculation procedure for the mass flow rate, the droplet temperature, and the composition at the liquid-gas interface and also in the liquid phase. In this work, a Newton iterative method has been used. The physical and transport properties of the liquid and the gas can be obtained from the estimation techniques and mixing rule as recommended by Reid et al.[51] From Eqs. 4 and 10, the evaporation mass flow rate and the heat flux from the gas phase to the droplet can be obtained. The liquid energy equation (Eq. 14) and the energy balance at the liquid-gas interface (Eq. 15) gives the new droplet temperature. The variation of droplet radius is evaluated using the droplet mass m_a^n. The new droplet radius (exponent $n+1$) is obtained by mass conservation:

$$r_d^{n+1} = \left(\frac{m_d^n - \dot{m}.\Delta t}{\frac{4}{3}\pi\rho_l} \right)^{1/3} \tag{28}$$

where Δt is the time step, and ρ_l is the UWS droplet density which is assumed to be constant in each time step. The density of urea is assumed to be constant. However, the density change of water in UWS droplet with the temperature is taken into account using Rackett's correlation.[51]

Kinetic modeling

The state of aggregation of urea after the evaporation of water and during the thermal decomposition remains largely unknown.[3] Kontin et al.[13] showed that the impact of oversaturation in UWS leading to urea precipitation can be significant at low temperatures. Consequently, urea can be present in different forms (solid, dissolved, molten) depending on the operating conditions.[52] Urea, biuret as well as CYA start decomposing before melting so that the existence of the molten phase is restricted to a quite narrow temperature window.[2,53] In this study, the reactions are supposed to take place in solid phase. The development and validation of the kinetic model was performed using the AURORA application of Chemkin 4.1 software[54] which allows the simulation of a continuous stirred tank reactor. However, complementary calculations using continuously stirred reactors (CSTR) in series were performed to investigate the impact of macromixing, which was found to be negligible in our case. This is not surprising because the reactants considered in the present kinetic model are exclusively condensed phase species. According to the mean-field approximation, the species are

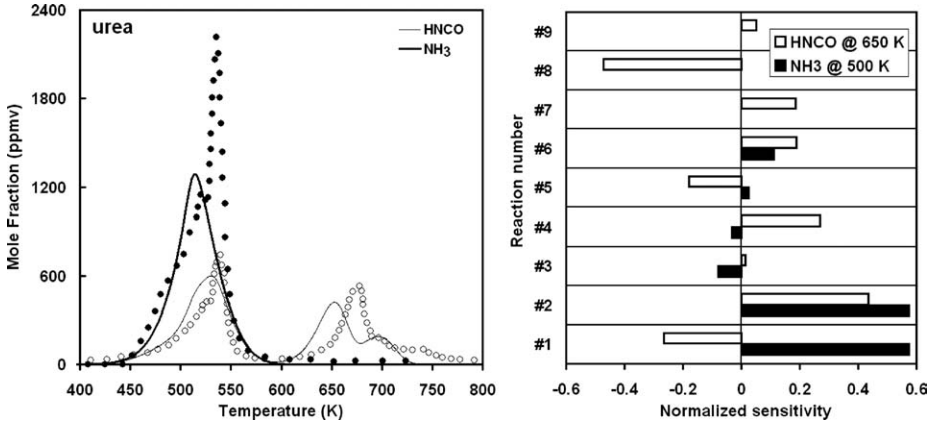

Figure 2. Case 1: (a) Comparison of modeling results (lines) with experimental concentration profiles (symbols) and (b) normalized sensitivity coefficients.

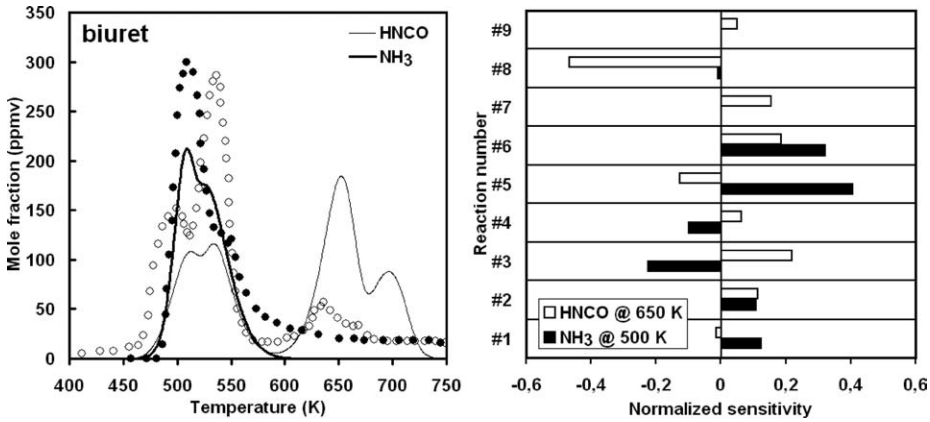

Figure 3. Case 2: (a) Comparison of modeling results (lines) with experimental concentration profiles (symbols) and (b) normalized sensitivity coefficients.

assumed to be randomly distributed on a uniform surface. The tetragonal lattice parameters of solid urea are 0.56 and 0.47 nm.[55] Considering a facet having an area of $(0.56\ \text{nm})^2$, an urea site density of 5.3×10^{-10} mol cm^{-2} is deduced. The net rate of formation of kth species is given by [56]:

$$r_k^{\text{reaction}} = \sum_{i=1}^{N\text{reactions}} \nu_{ki} A_i' \exp\left(-\frac{E_i}{RT}\right) \prod_{j=1}^{N\text{species}} Cs_j^{\nu_{ji}} \quad [\text{mol.cm}^{-2}.\text{s}] \tag{29}$$

where, ν_{ki} stands for the stoichiometric coefficient of the kth species in the ith reaction. $A_i^{'}$ and E_i are respectively the pre-exponential factor and activation energy of ith reaction and Cs_j is the surface concentration of jth species. $A_i^{'}$ is linked to the pre-exponential factors A_i of Table 2 via the site density Γ :

$$A_i' = \frac{A_i}{\Gamma^{ni-1}} \quad [\text{cm}^{2\text{ni}-2}.\text{mol}^{\text{ni}-1}.\text{s}^{-1}] \tag{30}$$

where n_i represents the ith reaction order. The active surface is calculated from

$$S = \sum_{k=1}^{N\text{species}} \frac{m_k^{\text{initial}} \sigma_k}{W_k \Gamma} \quad [\text{cm}^2] \tag{31}$$

where, σ_k corresponds to the number of sites occupied by each molecule of the kth species. W_k stands for the molecular weight of the kth species. The active surface S allows for the calculation of the chemical source term in the CSTR mass balance equation from the specific net rate of formation r_k according to $\frac{dY_k}{dt} = \frac{1}{\tau}\left(Y_k^{\text{in}} - Y_k\right) + \frac{r_k W_k S}{\rho V_r}$ where, τ corresponds to the mean residence time in the CSTR and V_r denotes the CSTR volume.

The kinetic scheme used in this study consists of 12 steps (see Table 2). The first nine steps are related to urea thermal decomposition in dry media, whereas the last three steps correspond to the thermal decomposition of urea obtained from UWS. It should be noted that the impact of pH on thermohydrolysis kinetics[57,58] was not considered in this study.

All rate constants were optimized independently to best match the experimental data given in Table 2. The optimization could be achieved because for each single operating condition, species concentration profiles are generally sensitive to a small set of rate constants and the range of conditions investigated allows complementary reaction sets to be brought into play (Figure 2–7). This can be quantitatively substantiated using normalized sensitivity coefficients S_{ij}[59] defined by $S_{ij} = \frac{A_i}{Cs_j}\frac{\partial Cs_j}{\partial A_i}$ where A_i corresponds to the preexponential factor of ith reaction and Cs_j is the surface concentration of jth species. For example, in case 3 (see Figure 4), urea concentration at 500 K is quasi exclusively sensitive to reaction R1.

The biuret decomposition to yield melt urea was considered to proceed in both directions (reactions R4 and R5). Thermodynamic consistency is guaranteed by computing the

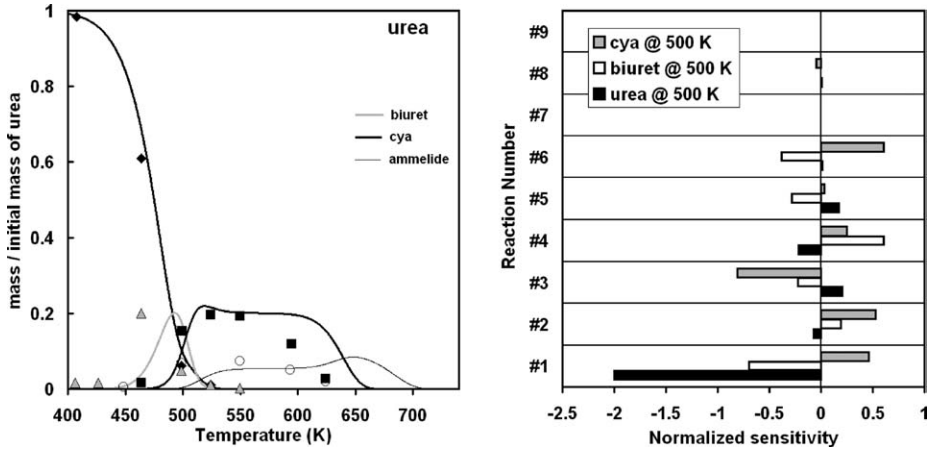

Figure 4. Case 3: (a) Comparison of modeling results (lines) with experimental concentration profiles (symbols) and (b) normalized sensitivity coefficients.

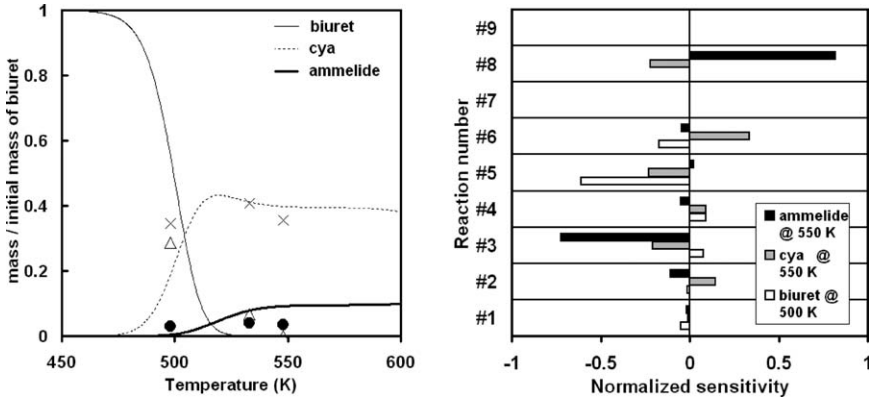

Figure 5. Case 4: (a) Comparison of modeling results (lines) with experimental concentration profiles (symbols) and (b) normalized sensitivity coefficients.

activation energy of R5 from that of R4 and the corresponding equilibrium constant. The backward steps corresponding to the other reactions were neglected for simplicity purposes. In particular, the adsorption of HNCO(g) or H_2O(g) was neglected in this modeling study. Indeed, the presence of H_2O in gas phase was shown to only slightly affect solid urea decomposition.[35] Reactions R1 and R10 involve "solid" and "aqueous" urea, which behave differently toward thermal decomposition.[60] Previous studies[61–63] indicate that the backward step of R1 can be of significance in our conditions. However, for simplicity purposes, we choose to include only the forward step of R1. The activation energies used in this modeling work for R1 and R10 are that recommended by Schoppelrei et al.[21] Schoppelrei et al.[22] find a pre-exponential factor ranging between 2.19×10^7 and 3.98×10^7 s^{-1} depending on the flow cell used. The optimized pre-exponential factors for R1 and R10 lie, respectively, slightly below and above the values obtained by Schoppelrei et al.[22] (see Table 2). The activation energy for NH_3(g) production from NH_4^+ (reaction R2) is close to the barrier of 41 kJ mol^{-1} reported by Donaldson.[64] Reaction R11 corresponds to the sum of reactions R11a, R11b, and R11c presented in the literature review. Rate data for this reaction are taken from Schoppelrei et al.[21] Reactions R6 to R8 rely on the findings of Schaber et al.[34] and Fang et al.[35] The activation energy of reaction R7 differs clearly from that proposed by Lédé et al.,[65] even if both corresponding rate constant values coincide at 647 K. This temperature lies in the range of conditions which is typical of CYA decomposition (see Figure 6). Note that the rate constant of Lédé et al.[65] was derived from experiments at temperatures higher than 700 K and that its applicability at lower temperatures is therefore not established. This issue is not critical in the present modeling but should deserve a dedicated study.

The present kinetic scheme was validated over a wide range of operating conditions (see Table 3). Figure 2–7 present the comparisons of modeling results with experimental data. Although mass loss to gas phase is slightly underpredicted for biuret thermolysis (cases 2 and 4), the overall agreement is good. The kinetics of biuret, cya, or heavier by-products can probably not be captured perfectly by a simple kinetic scheme involving only interactions with NCO^-. However, the kinetic model performs remarkably well for urea thermal decomposition (cases 1 and 3), which is the scope of this study. It should be also noted that complementary calculations were performed using a 3D code (IFP-C3D) leading to the same results.

Results and Discussion

Impact of urea aggregation state

As shown previously, the model is able to simulate well in various experimental concentration profiles. Therefore, we can perform with some confidence rate-of-reaction analyses to interpret the impact of operating conditions on urea thermal decomposition.

In case 7, the production of NCO^- by reaction R10 occurs at a lower temperature compared to case 1 (reaction R1).

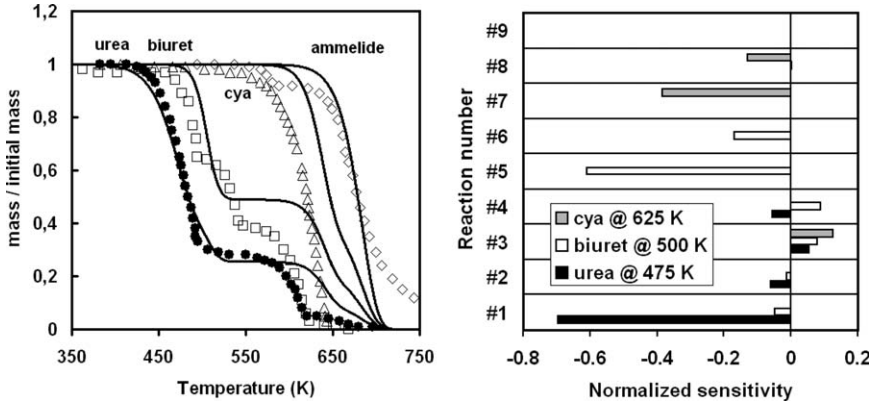

Figure 6. Cases 3–6: (a) Comparison of modeling results (lines) with experimental concentration profiles (symbols) and (b) normalized sensitivity coefficients.

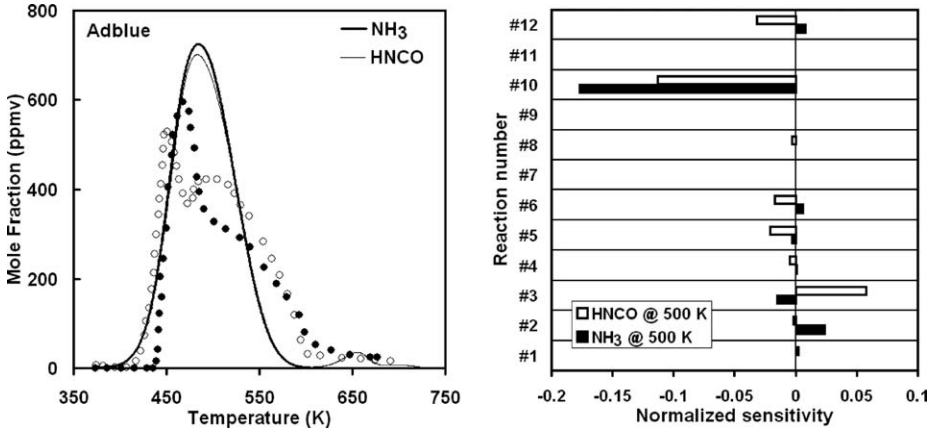

Figure 7. Case 7: (a) Comparison of modeling results (lines) with experimental concentration profiles (symbols) and (b) normalized sensitivity coefficients.

This 50-K shift results in the strong reduction of the extent of the pathways leading to polymeric compounds (see Figure 8). Rate analyses reveal that this effect is mainly due to the difference between the activation energies of R3 and R12 (or R3 and R4). As R3 has much lower activation energy than R12, the 50 K shift in urea consumption onset has a smaller impact on the corresponding rate constant. The maximum reaction rate of R12 in case 7 is 25 times smaller than the peak of R4 rate observed in case 1, whereas the R3 maximum rate is only affected by about 30%. It should be noted, however, that the concentration effect in the mass action law is very small since NCO^- and urea concentration profiles are shifted to the same extent, so that the product of these two concentrations remains nearly unaffected when replacing solid urea by Adblue.

Impact of heating rate

The impact of the slope of the temperature ramp (see Figure 9) has a similar explanation. In this case, the 10 K shift in urea decomposition onset is due to the thermal history of the material. This affects reactions R3 and R12 very differently (see Figure 9) due to the strong discrepancies between the corresponding activation energies. Consequently, the polymerization pathway contribution to urea consumption rate strongly decreases. This phenomenon provides an alternative, but not exclusive, explanation to that proposed by Lundström et al.,[60] namely that the increase of HNCO gas-phase concentration at higher heating rate can enhance polymerization. According to this result, it is preferable to operate at lower heat flow rates to avoid the formation of heavier byproducts.

Impact of gas-phase chemistry

The contribution of gas-phase chemistry in HNCO formation was also studied in the conditions of case 1 using the kinetic scheme of Glarborg et al.[66] As can be noticed on Figure 10, a slight impact of gas-phase kinetics can be noticed at the higher edge of the temperature range investigated. HNCO spontaneous decomposition kinetics is rather slow in the temperature range investigated.[68,69] Therefore, the thermal decomposition of HNCO should be triggered by an active species produced by ammelide decomposition. The slight decrease in HNCO concentration is found to be quasi exclusively due to the following reaction:

$$H + HNCO \rightarrow NH_2 + CO \text{ (normalized rate of consumption of 98.9\% at 700 K)} \quad (32)$$

This result is in line with the major reaction pathways reported by Glarborg et al.[66] According to Glarborg's mechanism, the H radicals are mainly produced by the following reactions

$$NH + NH \rightarrow N_2 + H + H(58\% \text{ at } 700\text{ K}) \quad (33)$$

$$NH + N \rightarrow N_2 + H(35\%) \quad (34)$$

and consumed by

$$NH_2 + H + M \rightarrow NH_3 + M\ (18\% \text{ at } 700\text{ K}) \quad (35)$$

$$NH + H \rightarrow N + H_2\ (43\%) \quad (36)$$

$$N_2H_2 + H \rightarrow N_2H_3\ (15\%) \quad (37)$$

Table 3. Experimental Setups Used for the Validation of the Kinetic Model

Validation case	Volume (cm^3)	Flow rate ($Ncm^3\ s^{-1}$)	Reactant	Temperature ramp ($K\ s^{-1}$)	Modeling code
1[60]	0.054 (cup)	1.67	0.9 mg urea	0.333	Chemkin 4.1[54] IFP-C3D[50]
2[60]	0.054 (cup)	1.67	0.25 mg biuret	0.333	Chemkin 4.1
3[34]	10 (reactor)	1.00*	30 mg urea	0.167*	Chemkin 4.1
4[34]	10 (reactor)	1.00*	30 mg biuret	0.167*	Chemkin 4.1
5[34]	10 (reactor)	1.00*	30 mg cyanuric acid	0.167*	Chemkin 4.1
6[34]	10 (reactor)	1.00*	30 mg ammelide	0.167*	Chemkin 4.1
7[60]	0.044 (monolith)	1.67	2.46 mg Adblue	0.333	Chemkin 4.1
8[60]	0.044 (monolith)	1.67	2.46 mg Adblue	0.167	Chemkin 4.1 IFP-C3D

*Schaber PM. *Private communication*. 2010.

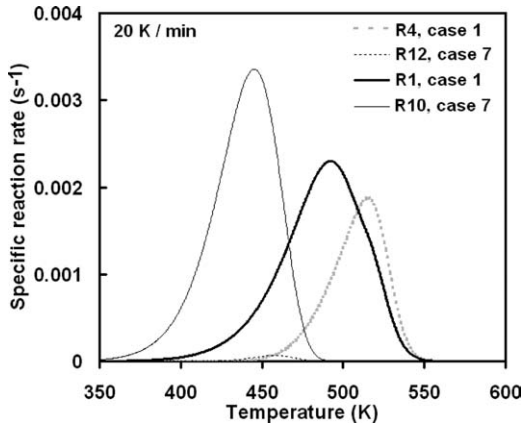

Figure 8. Comparison of specific reactions rates predicted in cases 1 and 7.

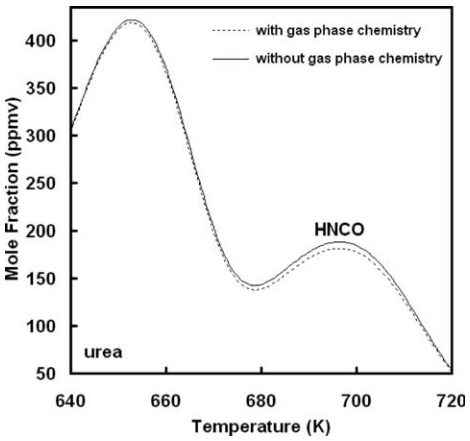

Figure 10. Case 1: Impact of gas phase chemistry[67] on HNCO concentration profile.

$$HNCO + H \rightarrow NH_2 + CO \ (12\%) \qquad (38)$$

It should be reminded that gas-phase consumption of HNCO is dependent on the formulation of reaction R9. This result claims, therefore, for further investigation of ammelide decomposition chemistry.

Isolated droplet evaporation

The effect of urea on the evaporation of water from UWS (32.5% wt. urea in water) is studied using the UWS-NRTL model. An isolated UWS droplet with the initial diameter and temperature of 100 μm and 293 K is putted on the center of a cube. The stagnant gas consists of nitrogen with the temperature of 673 K and pressure of 1 bar. The results of the model are compared with the numerical results of Kontin et al.[13] for the same conditions. The results of droplet evaporation are illustrated in Figure 11. Figure 11a shows the dimensionless droplet mass. Compared to pure water, the results of Kontin et al.[13] show a higher evaporation rate. The new UWS-NRTL model shows a slightly lower evaporation than the pure water case. This result is qualitatively in accordance with the experiments.[14] The difference in mass evaporation rate is due to the presence of urea in UWS. Urea affects the vapor pressure of UWS which leads to the reduction in the mass transfer. As the NRTL model is used, decrease in the vapor pressure of UWS leads to the decrease in the mass evaporation rate and increase in droplet temperature. Figure 11b shows the droplet temperature as a function of urea percentage in the droplet. Having similar heat flux from the gas to the liquid for both pure water and UWS droplets, NRTL model predicts a higher droplet temperature. In fact, the heat flux to the UWS droplet is more dedicated to heat up the droplet than to evaporate it. This behavior is well presented in both Figure 11a, b. Figure 11b also shows that the UWS droplet temperature exceeds the saturation temperature of the water. This temperature increase could be attributed to the lower vapor pressure of UWS and consequently higher saturation temperature than pure water. The Figure 11b also shows that the "UWS temperatures curve" crosses the "UWS equilibrium curve" at a urea concentration close to 0.77 and enters the "solid-liquid" two-phase region. In this case, the suggested model assumes that urea is still dissolved (i.e., UWS becomes overdissolved with urea) until the total evaporation of water. The mass fraction of water and urea in UWS droplet is shown in Figure 11c. As water evaporates from UWS droplet, its contribution in droplet decreases (Figure 11c). The saturation temperature of the UWS then increases by increasing the urea percentage in UWS. According to Figure 11d, the UWS-NRTL model predicts a higher droplet temperature compared to the pure water. The effect of urea on UWS droplets temperature (Figure 11d) seems to be more important that its effect on water evaporation (Figure 11a). As the decomposition of urea is highly related to the droplet temperature, an inaccurate value of temperature may lead to the uncertainties in the decomposition behavior. Hence, the UWS-NRTL model allows to accurately calculating the droplet temperature to be

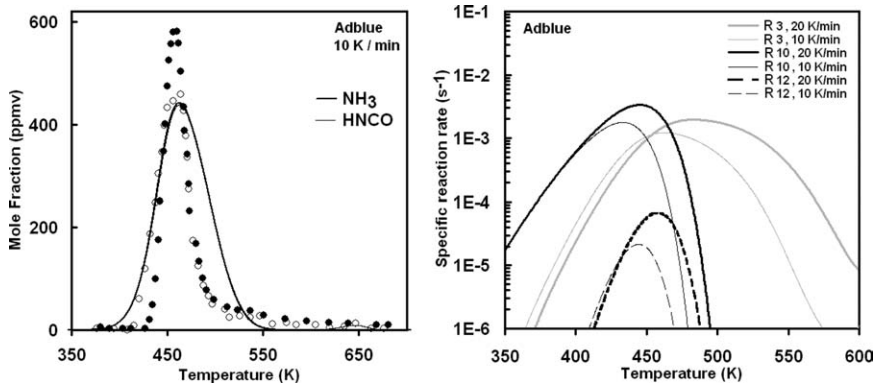

Figure 9. Case 8: (a) Comparison of modeling results (lines) with experimental concentration profiles (symbols) and (b) comparison of specific reaction rates obtained in cases 7 and 8.

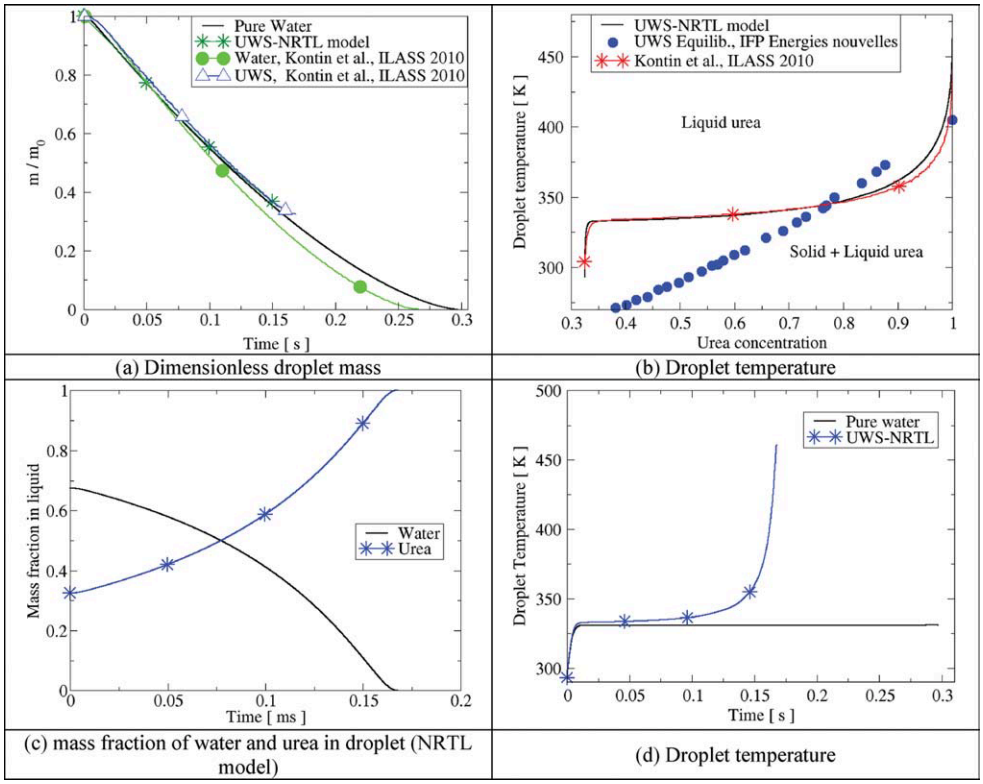

Figure 11. Comparison of water droplet vaporization with (NRTL model) and without (pure water) presence of urea.

The experimental data are extracted from Ref. 13. (a) Dimensionless droplet mass, (b) droplet temperature, (c) mass fraction of water and urea in droplet (NRTL model), and (d) droplet temperature. [Color figure can be viewed in the online issue, which is available at wileyonlinelibrary.com.]

used in the thermal decomposition of urea. According to Figure 11a, water evaporation from UWS continues until it reaches the 32.5% of the droplet mass. The remaining mass in UWS droplet is assumed to correspond to the mass of solid/molten urea.

Conclusions and Future Work

In this study, a model accounting for both UWS evaporation and thermal decomposition has been developed. The UWS evaporation submodel takes into account the nonideality of UWS due to the dissolved urea. The vapor pressure of UWS is obtained from Raoult's law using the NRTL activity model. The semidetailed kinetic submodel relies on the mean-field approximation and describes the evolution of the main reaction products as well as the production and consumption of biuret, CYA, and ammelide. This submodel has been validated against a wide range of experimental data on urea thermal decomposition. Both evaporation and kinetic model have been implemented on *IFP-C3D* CFD code. The results obtained reveal a slight effect of urea on the water evaporation but a significant effect of UWS temperature especially near the end of the water evaporation. Overall, the agreement between model prediction and experimental species profiles is found to be very good. In line with the experimental data, lower heating rates cause HNCO production to occur at the lower temperatures. It is also predicted that reducing the heating rate causes the importance of the polymerization pathway to decrease as a result of its higher activation energy than that of the direct urea decomposition pathway. The contribution of the hydrolysis pathway is found to be of minor importance under the operating conditions investigated. The contribution of gas-phase chemistry is found to be insignificant for temperatures lower than 700 K. Further investigations on the presence of residual water in urea resulting from complete evaporation[70] are needed. In addition, the suggested models are going to be validated with UWS spray droplets in conditions representative of actual SCR systems using for instance, the recently published experimental results by Wang et al.[71]

Acknowledgments

The authors thank Schaber as well as Lundström for providing additional information on their experimental setups. Vahid Ebrahimian thanks IFPEN for providing a doctoral grant.

Literature Cited

1. Held W, König A, Richter T, Puppe L. Catalytic NOx reduction in net oxidizing exhaust gas. SAE International, Paper No. 900496, 99, SAE International Congress and Exposition, Detroit, MI 1990.
2. Koebel M, Elsener M, Kleemann M. Urea-SCR: a promising technique to reduce NOx emissions from automotive diesel engines. *Catal Today*. 2000;59:335–345.
3. Birkhold F, Meingast U, Wassermann P, Deutschmann O. Modeling and simulation of the injection of urea-water-solution for automotive SCR DeNOx-systems. *Appl Catal B: Environ*. 2007;70:119–127.
4. Grünwald JD. *Verbesserung der Reduktionsmitteldispersion und verdunstung in SCR-Abgasanlagen*. Technische Universität München, 2007.
5. Nomura H, Ujiie Y, Rath HJ, Sato J, Kono M. Experimental study on high-pressure droplet evaporation using microgravity conditions. *Sympos(Int) on Combust*. 1996;26:1267–1273.
6. Chauveau C, Halter F, Lalonde A, Gokalp I. *An experimental study on the droplet vaporization: effects of heat conduction through the support fiber*. *IT 2008*, ILASS-EUROPE, COMO, Italy, 2008; 8–10.

7. Abramzon B, Sirignano WA. Droplet vaporization model for spray combustion calculations. *Int J Heat Mass Transfer*. 1989;32:1605–1618.
8. Sazhin S. Advanced models of fuel droplet heating and evaporation. *Prog Energy Combust Sci*. 2006;32:162–214.
9. Ra Y, Reitz RD. A vaporization model for discrete multi-component fuel sprays. *Int J Multiphase Flow*. 2009;35:101–117.
10. Ebrahimian V, Habchi C. Towards a predictive evaporation model for multi-component hydrocarbon droplets at all pressure conditions. *Int J Heat Mass Transfer*. 2011;54:3552–3565.
11. Basu S, Cetegen BM. Modeling of thermo-physical processes in liquid ceramic precursor droplets injected into a plasma jet. *Int J Heat Mass Transfer*. 2007;50:3278–3290.
12. Herr A. *Thermische Zersetzung von Festharnstoff für mobile SCR-Katalysatoranwendungen*. Technischen Universität Kaiserslautern, 2004.
13. Kontin S, Höfler A, Koch R, Bauer H-J. Heat and mass transfer accompanied by crystallisation of single particles containing urea-water solution. ILASS-Europe 2010, 23rd Annual Conference on Liquid Atomization and Spray Systems, Brno, Czech Republic, 2010.
14. Musa SNA., Saito M, Furuhata T, Arai M. *evaporation characteristics of a single aqueous urea solution droplet*. ICLASS 2006, Kyoto, Japan, 2006.
15. Faeth GM. Evaporation and combustion of sprays. *Prog Energy Combust Sci*. 1983;9:1–76.
16. Sirignano WA. Fuel droplet vaporization and spray combustion theory. *Prog Energy Combust Sci*. 1983;9:291–322.
17. Reinhold M. *Theoretische und experimentelle Untersuchung zur Sprühtrocknung mit Überlagerung chemischer Reaktion*. Technische Universität Clausthal, Shaker. 2001.
18. Abu-Ramadan E, Saha K, Li X. Modeling the depleting mechanism of urea-water-solution droplet for automotive selective catalytic reduction systems. *AIChE J*. 2011; DOI 10.1002/aic.12523.
19. Zheng G, Fila A, Kotrba A, Floyd R. Investigation of urea deposits in urea SCR systems for medium and heavy duty truck. SAE International, Paper No 2010–01–1941, SAE Commercial Vehicle Engineering Congress, Chicago, IL, 2010.
20. Eichelbaum M, Farrauto RJ, Castaldi MJ. The impact of urea on the performance of metal exchanged zeolites for the selective catalytic reduction of NOx: part I. pyrolysis and hydrolysis of urea over zeolite catalysts. *Appl Catal B: Environ*. 2010;97:90–97.
21. Kieke ML., Schoppelrei JW, Brill TB. Spectroscopy of hydrothermal reactions. 1. The CO_2-H_2O system and kinetics of urea decomposition in an FTIR spectroscopy flow reactor cell operatable to 725 K and 335 bar. *J Phys Chem*. 1996;100:7455–7462.
22. Schoppelrei JW, Kieke ML, Wang X, Klein MT, Brill TB. Spectroscopy of hydrothermal reactions. 4. Kinetics of urea and guanidinium nitrate at 200–300°C in a diamond cell, infrared spectroscopy flow reactor. *J Phys Chem*. 1996;100:14343–14351.
23. Okazaki M, Funazukuri T. Decomposition of urea in sub- and supercritical water with/without additives. *J Mater Sci*. 2008;43:2316–2322.
24. Takebayashi Y, Yoda S, Sugeta T, Otake K. *Continuous-flow reactor for kinetic analysis of rapid hydrothermal reactions by raman spectroscopy. 14th International Conference on the Properties of Water and Steam in Kyoto*. Kyoto, Japan. 2005; 440–444.
25. Alexandrova AN, Jorgensen WL. Why urea eliminates ammonia rather than hydrolyzes in aqueous solution. *J Phys Chem B*. 2007;111:720–730.
26. Birkhold F, Meingast U, Wassermann P, Deutschmann O. Analysis of the injection of urea-water-solution for automotive SCR DeNOx-systems: modeling of two-phase flow and spray/wall-interaction. SAE Paper No. 2006–01–0643, SAE International, SAE World Congress, Detroit, MI 2006.
27. Chen Z-C, Yang W-J, Zhou J-H, LV H-K, Liu J-Z, Cen K-F. HNCO hydrolysis performance in urea-water solution thermohydrolysis process with and without catalysts. *J Zhejiang Univ–Sci A (Appl Phys Eng)*. 2010;11:849–856.
28. Belson DJ, Strachan AN. Preparation and properties of isocyanic acid. *Chem Soc Rev*. 1982;11:41–56.
29. Aigner M, Zeilinger M, Hofbauer H. Kinetic study of the hydrolysis of isocyanic acid in the gas phase. *Chem Eng Proc*. 1995;34:515–520.
30. Schoppelrei JW, Kieke ML, Brill TB. Spectroscopy of hydrothermal reactions. 2. reactions and kinetic parameters of $[NH_3OH]NO_3$ and equilibria of $(NH_4)_2CO_3$ determined with a flow cell and FT Raman spectroscopy. *J Phys Chem*. 1996;100:7463–7470.
31. Kemp IA, Kohnstam G. The decomposition of inorganic cyanates in water. *J Chem Soc*. 1956; 900–911.
32. Tolosa Arroyo T, Hidalgo Garcia A, Sanson Martin JA. Theoretical study of the neutral hydrolysis of hydrogen usocyanate in aqueous solution via assisted-concerted mechanisms. *J Phys Chem A*. 2009;113:1858–1864.
33. Chen JP, Isa K. Thermal Decomposition of Urea and Urea Derivatives by Simultaneous TG/(DTA)/MS. *J Mass Spectrom Soc Jpn*. 1998;46:299–303.
34. Schaber PM, Colson J, Higgins S, Thielen D, Anspach B, Brauer J. Thermal decomposition (pyrolysis) of urea in an open reactino vessel. *Thermochimica Acta*. 2004;424:131–142.
35. Fang HL, DaCosta HFM. Urea thermolysis and NOx reduction with and without SCR catalysts. *Appl Catal B: Environ*. 2003;46:17–34.
36. Alzueta MU, Bilbao R, Millera A, Oliva M, Ibanez JC. Interactions between nitric oxide and urea under flow reactor conditions. *Energy Fuels*. 1998;12:1001–1007.
37. Tokmakov IV, Alavi S, Thompson DL. Urea and urea nitrate decomposition pathways: a quantum chemistry study. *J Phys Chem A*. 2006;110:2759–2770.
38. Giovangigli V. *Multicomponent Flow Modeling*. Boston: Birkhäuser, 1999.
39. Poinsot T, Veynante D. *Theoretical and Numerical Combustion*. Philadelphia: Edwards, Inc., 2005.
40. Hirschfelder JO, Curtiss CF, Bird RB. *Molecular Theory of Gases and Liquids*. 1954; New York: John Wiley and Sons.
41. Hubbard GL, Denny VE, Mills AF. Droplet evaporation: Effects of transients and variable properties. *Int J Heat Mass Transfer*. 1975;18:1003–1008.
42. Lefèbvre C, Lugo R. Calcul des pressions de vapeur de mélanges eau-urée pour des températures situées entres 300 K et la température critique de l'eau par le modèle NRTL. Internal Technical Note IFP Energies nouvelles, R0740R-CL-RL/sg No. 269, Rueil-Malmaison, France 2010.
43. Desoutter G, Habchi C, Cuenot B, Poinsot T. *Single-component Liquid film evaporation model development and validation using Direct Numerical Simulation*. ICLASS, Kyoto, 2006.
44. Dryer FL. *Water addition to practical combustion systems—concepts and applications. 16th International Symposium on Combustion*, The Combustion Institute, Pittsburgh, PA. 1977, p 279.
45. Glarborg P, Kubel D, Kristensen PG, Hansen J, Dam-Johansen K. Interactions of CO, NO_x and H_2O under post-flame conditions. *Combust Sci Technol*. 1995;110:461–485.
46. Hohmann S, Renz U. Numerical simulation of fuel sprays at high ambient pressure: the influence of real gas effects and gas solubility on droplet vaporisation. *Int J Heat Mass Transfer*. 2003;46:3017–3028.
47. Kulmala M, Vesala T. Mass transfer from a drop—II. theoretical analysis of temperature dependent mass flux correlation. *Int J Heat Mass Transfer*. 1995;38:1705–1708.
48. VIDAL J. *Thermodynamics: Applications in Chemical Engineering and the Petroleum Industry*. Paris: IFP, 2003.
49. *DIPPR database, Project 801 Evaluated Thermophysical Property Database. V 4.0.0*. Available at: http://www.aiche.org/dippr/.
50. Bohbot J, Gillet N., Benkenida A. IFP-C3D: an unstructured parallel solver for reactive compressible gas flow with spray. *Oil Gas Science Technology-Revue de l Institut Francais du Petrole*. 2009;64:309–335.
51. Reid RC, Prausnitz JM, Poling BE. *The Properties of Gases and Liquids*. New York: McGraw-Hill, 1988.
52. Wang XZ, Ma CY. Morphological population balance model in principal component space. *AIChE J*. 2009;55:2370–2381.
53. Schmidt A. Verfahrenstechnische Probleme bei der Herstellung von Melamin aus Harnstoff bei Atmospharendruck. *Österr Chemiker-Ztg*. 1967;68:175–179.
54. Kee RJ, Rupley FM, Miller JA, Coltrin ME, Grcar JF, Meeks E, Moffat HK. Lutz AE, Dixon-Lewis G, Smooke MD, Warnatz J, Evans GH, Larson RS, Mitchell RE, Petzold LR, Reynolds WC, Caracotsios M, Stewart WE, Glarborg P, Wang C, McLellan CL, Adigun O, Houf WG, Chou CP, Miller SF, Ho P, Young PD, Young DJ, Hodgson DW, Petrova MV, Puduppakkam KV. *CHEMKIN Release 4.1*. San Diego, CA: Reaction Design, 2006.
55. Xue D, Zhang S. Chemical bond analysis of nonlinearity of urea crystal. *J Phys Chem A*. 1997;101:5547–5550.
56. Coltrin ME, Kee RJ, Rupley FM. *SURFACE CHEMKIN: A Fortran Package for Analyzing Heterogeneous Chemical Kinetics at a Solide-Surface—Gas-Phase Interface*. SAND90–8003B, Livermore, 1991.
57. Shaw WHR, Bordeaux JJ. The decomposition of urea in aqueous media. *J Am Chem Soc*. 1955;77:4729–4733.

58. DeMartini N. *Conversion Kinetics for Smelt Anions: Cyanate and Sulfide*. Abo Akademi University; 2004.
59. Aghalayam P, Park YK, Valchos DG. Construction and optimization of complex surface-reaction mechanisms. *AIChE J*. 2000;46: 2017–2029.
60. Lundström A, Andersson B, Olsson L. Urea thermolysis studied under flow reactor conditions using DSC and FT-IR. *Chem Eng J*. 2009;150:544–550.
61. Raunier S, Chiavassa T, Marinelli F, Aycard J-P. Experimental and theoretical study on the spontaneous formation of OCN^- ion: reactivity between HNCO and NH_3/H_2O environment at low temperature. *Chem Phys*. 2004;302:259–264.
62. Brooker MH, Wen N. Raman studies of cyanate: Fermi resonance, hydration and hydrolysis to urea. *Can J Chem*. 1993;71:1764–1773.
63. Wen N, Brooker MH. Rate constants for cyanate hydrolysis to urea: a Raman study. *Can J Chem*. 1994;72:1099–1106.
64. Donaldson DJ. Adsorption of atmospheric gases at the air-water interface. I. NH3. *J Phys Chem A*. 1999;103:62–70.
65. Lédé J, Mercadier J. Simulation of the thermal cracking of biomass derived vapours, by the model reaction of decomposition of isocyanuric acid. *J Anal Appl Pyrolysis*. 2003;67:295–305.
66. Glarborg P, Kristensen PG, Jensen SH, Dam-Johansen K. A flow reactor study of HNCO oxidation chemistry. *Combust Flame*. 1994;98:241–258.
67. Mendiara T, Glarborg P. Ammonia chemistry in oxy-fuel combustion of methane. *Combust Flame*. 2009;156:1937–1949.
68. Back RA, Childs J. Pyrolysis of HNCO vapor. *Can J Chem*. 1968;46:1023–1024.
69. He Y. Liu X, Lin M.C. Melius CF. The thermal reaction of HNCO at moderate temperatures. *Int J Chem Kinet*. 1991;23:1129–1149.
70. Lee C, Stahlberg EA, Fitzgerald G. Chemical structure of urea in water. *J Phys Chem*. 1995;99:17737–17741.
71. Wang TJ, Baek SW, Lee SY, Kang DH, Yeo GK. Experimental investigation on evaporation of urea-water-solution droplet for SCR applications. *AIChE J*. 2009;55:3267–3276.

Manuscript received May 5, 2011, and revision received Jun. 20, 2011.